JOURNAL OF CHEMICAL INFORMATION AND MODELING

Article

pubs.acs.org/jcim

Modeling the Closed and Open State Conformations of the $GABA_A$ Ion Channel - Plausible Structural Insights for Channel Gating

R. S. K. Vijayan,[†,∥] Neha Trivedi,[‡] Sudipendra Nath Roy,[‡] Indrani Bera,[†] Prabu Manoharan,[†] Pavan V. Payghan,[†] Dhananjay Bhattacharyya,[§] and Nanda Ghoshal*[,†]

[†]Structural Biology and Bioinformatics Division, CSIR - Indian Institute of Chemical Biology, Kolkata −700 032, India

[‡]National Institute of Pharmaceutical Education and Research, Kolkata −700 032, India

[§]Computational Science Division, Saha Institute of Nuclear Physics, Kolkata −700 064 India

Supporting Information

ABSTRACT: Recent disclosure of high resolution crystal structures of *Gloeobacter violaceus* (GLIC) in open state and *Erwinia chrysanthemii* (ELIC) in closed state provides newer avenues to advance our knowledge and understanding of the physiologically and pharmacologically important ionotropic $GABA_A$ ion channel. The present modeling study envisions understanding the complex molecular transitions involved in ionic conductance, which were not evident in earlier disclosed homology models. In particular, emphasis was put on understanding the structural basis of gating, gating transition from the closed to the open state on an atomic scale. Homology modeling of two different physiological states of $GABA_A$ was carried out using their respective templates. The ability of induced fit docking in breaking the critical inter residue salt bridge (Glu155β_2 and Arg207β_2) upon endogenous GABA docking reflects the perceived side chain rearrangements that occur at the orthosteric site and consolidate the quality of the model. Biophysical calculations like electrostatic mapping, pore radius calculation, ion solvation profile, and normal-mode analysis (NMA) were undertaken to address pertinent questions like the following: How the change in state of the ion channel alters the electrostatic environment across the lumen; How accessible is the Cl^- ion in the open state and closed state; What structural changes regulate channel gating. A "Twist to Turn" global motion evinced at the quaternary level accompanied by tilting and rotation of the M2 helices along the membrane normal rationalizes the structural transition involved in gating. This perceived global motion hints toward a conserved gating mechanism among pLGIC. To paraphrase, this modeling study proves to be a reliable framework for understanding the structure function relationship of the hitherto unresolved $GABA_A$ ion channel. The modeled structures presented herein not only reveal the structurally distinct conformational states of the $GABA_A$ ion channel but also explain the biophysical difference between the respective states.

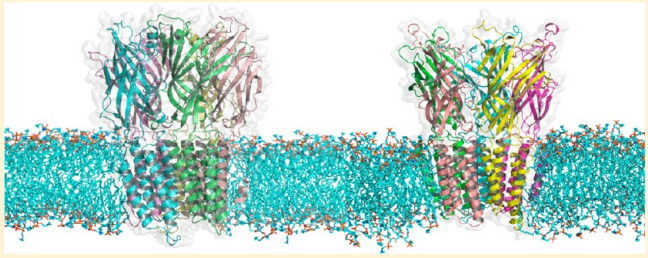

INTRODUCTION

Gamma amino butyric acid (GABA) is the predominant inhibitory neurotransmitter that counteracts the excitatory glutamatergic neurotransmission in the mammalian system.[1] GABA exerts its physiological effects by binding to the ionotropic ($GABA_A$, $GABA_c$) and the metabotropic ($GABA_B$) receptors.[2,3] Of these, the anion selective ($GABA_A$) ionotropic receptor ($GABA_AR$) is the major inhibitory neuronal receptor of the mammalian brain conferring fast synaptic inhibition. $GABA_AR$ has also received the greatest attention in terms of research because of its importance as a pharmacological target for many clinically important drugs like barbiturates, neurosteroids, loreclezole, anesthetics, ethanol, and benzodiazepines (BDZs).[4] $GABA_AR$ exhibits varied heterogeneity and is assembled from a repertoire of at least 21 subunits evolved within 8 families (α_{1-6}, β_{1-4}, γ_{1-4}, 1δ, 1ε, 1π, 1θ, and ρ_{1-3}).[5] The finding that multiple receptor subunits are expressed within a single neuron reveals the complex and heterogeneous nature of the receptor.

This ionotropic $GABA_A$ receptor is a membrane bound pore forming hetropentameric complex, arranged pseudosymmetrically around a central Cl^- selective ion channel. Historically, they have been referred to as 'Cys-loop receptors' and belong to a super family of pentameric ligand-gated ion channels (pLGICs).[6] The N-terminal, extracellular domain (ECD) possesses a hallmark Cys loop, formed by two canonical cysteine residues constituting a disulfide bridge intervened by 13 amino acids.

Structural investigations on $GABA_A$ receptor are precluded due to a host of issues such as large size (~50 kD), heterogeneity, low abundance (pmol/mg of protein), together with other inherent difficulties associated in isolation and purification of integral membrane proteins.[7] Fortunately, the availability of the crystal structure of nicotinic acetylcholine receptor (nACh) at reasonable resolution[8] has proven to be

Received: April 18, 2012
Published: November 1, 2012

providential and has been utilized by various groups to model the extracellular domain (ECD) and also to construct models inclusive of both ECD and transmembrane (TM) domain.[9−13]

Modeling studies have revealed the ECD topology of $GABA_AR$ to be predominantly composed of β-sheets. The ECD region of each subunit traverses down to the TM region forming a four α-helical TM bundle, with the helices designated as M1-M4. The loop connecting the helices M3 and M4 is very long, partially resolved, and is speculated to traverse down to the intracellular domain.

Recently resolved X-ray crystallographic structures of pentameric ligand-gated ion channel proteins of *Gloeobactar violaceus* (3EAM)[14] at 2.9 Å resolution, apparently in an open conformation, and another structure of *Erwinia chrysanthemi* (2VL0)[15] at 3.3 Å resolution, in a presumed closed conformation, could serve as potential templates to broaden our knowledge of the $GABA_A$ ion channel.

The present comparative modeling study, undertaken on the $GABA_A$ ion channel, distinguishes itself from earlier homology modeling studies, as it provides newer perspectives on relating structure with function on an atomic scale. In an attempt to delineate the intricate phenomenon of ion conduction and receptor activation involving channel opening, various biophysical calculations were undertaken.

MATERIALS AND METHODS

Comparative Modeling. Amino acid sequences of human $GABA_A\alpha_1$ (P14867), β_2 (P47870), and γ_2 (P18507) were retrieved from the UniProtKB database.[16] The signaling peptide part was edited, and the mature protein sequence was used for modeling. All subsequent amino acid numbering is based on the mature sequence without the signal peptide. A BLAST[17] search carried out against the Protein Data Bank (PDB) retrieved many pLGICs as hits. The hits retrieved were chosen, based on various criteria (R, R_{free}) and orientation of the subunits in a clockwise fashion (SI 1) leading to the choice of *Erwinia chrysanthemi* (2VL0) and *Gloeobactar violaceus* (3EAM) as best templates for modeling the closed and the open states, respectively. The percent sequence identity of the template and the target in terms of their respective subunits is provided in Table 1, and a view of sequence alignment is provided in the Supporting Information (SI 2). Despite the fact that the sequence identity between the template and the target falls in the twilight zone, it is experimentally established that all members of the pLGIC super family of ion channels adopt similar 3D folds. Hence, a profile based alignment protocol was employed using FUGUE.[18]

Table 1. Percentage Identity with Templates for Each Chain

template	chain α1	chain β2	chain γ2
3EAM (for open)	29.63%	30.68%	29.63%
2VL0 (for closed)	27.51%	31.21%	30.15%

Profile based alignment methods are based on the premise that structure is more conserved than sequence and hence more suited when sequence identity falls outside the realms of the "safe zone". The long intracellular loop present in all the subunits, connecting M3-M4, whose topology is unresolved, was replaced with seven glycine residues, as previous studies have revealed that seven glycines do not perturb the topology of a helix−loop−helix motif.[19]

A multichain modeling technique incorporating symmetry information was employed using the Modeller module of Accelrys Discovery studio 2.5 software.[20] Such a modeling approach offers the advantage of incorporating additional spatial restraints arising from subunit interfaces, together with disulfide restraints for the Cys-loop.

Atomic coordinates of the regions, structurally aligned with the template, were generated using a spatial restraint-based modeling approach.[21] The intervening loops and regions lacking equivalent atoms in the templates were generated using the internal coordinates approach employing the CHARMM topology library. The rotamers of amino acid side chains were optimized using a CHARMM[22] based energy minimization. A total of five models were generated, and the best model was chosen, based on Probability Density Function (PDF) and Discrete Optimized Protein Energy (DOPE)[23] scores. A PDF score signifies a pseudoenergy objective function, and a DOPE score is a statistical potential function based score.

The obtained models were subjected to molecular mechanics based energy refinement using an cvff22 force field, employing 2000 steps of Steepest Descent followed by 5000 steps of the Polak Ribiere Conjugate Gradient method keeping the backbone restrained, using force constant. Energy minimization was carried out using the Discover module of Insight II[24] using an implicit distance dependent dielectric solvent model. Subsequently, the modeled structures were evaluated for stereochemical accuracy, fold reliability, and packing quality, using Procheck,[25] Whatif,[26] and Profile-3D.[27]

Model Validation Using Molecular Dynamics Simulation. All atom molecular dynamic simulation of the refined structures was carried out with Gromacs 4.5.3[28] to check the overall structural stability, using the GROMOS 53a6[29] force field and the SPC[30] water model. The protein structures were embedded into a pre-equilibrated lipid bilayer of 128 POPC[31] (1-palmitoyl-2-oleoyl-phosphatidylcholine) molecules. The system was neutralized by addition of Na^+ and Cl^- counterions, maintaining the final salt concentration of 0.10 M and then energy minimized, initially by 5000 steps of steepest descent followed by conjugate gradient. An equilibration run of 500 ps was performed at the NPT ensemble by restraining the protein atoms and employing PBC. In the next stage, all restraints were removed, and a 5 ns MD simulation was carried out. The Nose-Hoover thermostat[32] was applied to maintain constant temperature of 323 K with 0.2 ps time constant. The Parrinello−Rahman barostat,[33] with uniform semi-isotropic scaling, was used at a pressure of 1 bar with 0.5 ps time constant. Long range electrostatic interactions were treated with the particle mesh Ewald algorithm.[34] Distance cut off for Coulombic and Lennard-Jones interactions was kept at 1.2 nm. To imply constraints on bonds, the LINCS algorithm[35] was used. Newton's equation of motion was integrated at a time step of 2 fs using the leapfrog algorithm. The coordinates of all atoms were saved every 2 ps. For both open and closed states, trajectories of 5 ns were analyzed.

Ligand Based Model Validation Using an Induced Fit Docking (IFD) Approach. Ligand supported validation of homology modeling is gaining immense popularity as a strategy to attain a higher degree of accuracy in homology modeling.[36−39] We carried out an induced fit docking approach employing the IFD module of Schrödinger.[40]

Initial geometries of the endogenous ligand γ-amino butyric acid (GABA) were modeled using Hyperchem7.5[41] and energy

optimized employing a semiempirical (PM3) level of theory. Standard preprocessing tools like Ligprep and protein preparation wizards of Schrödinger software were used to preprocess the ligand and protein, respectively, before undertaking docking. Proper rotamers were assigned for the terminal amide group of Asn and Gln. The ionization states for the acidic and basic groups were assigned assuming a biological pH. A restrained minimization was performed, using the OPLS-2005 force field, to optimize the hydrogen bonding interaction network until an RMSD convergence criteria of 0.30 Å for the heavy atoms was attained. An equally spaced 2 Å grid of dimensions 12 × 12 × 12 Å was generated against the centroid, defining binding site points (Arg119(α_1), Glu182(α_1), Asp183-(α_1), Tyr97(β2), Glu155(β2), Ser156(β2), Tyr157(β2), Phe200(β2)), for the endogenous GABA site so as to permeate the orthosteric site. A soft potential docking using a scaled van der Waals (vdW) radius of 0.5 and partial charge cutoff of 0.25 was used for initial docking using the Glide[42] SP mode. Each of the resulting top 20 poses, as ranked by Glide score, were subjected to a full cycle of Prime[43] refinement using OPLS parameter sets. Residues within 13 Å from the grid center were treated as flexible, and those beyond this zone were kept rigid. The resulting energy minimized complexes were then used to redock the ligands using the Glide extra precision (XP) mode using a hard potential function (vdW scaling 1). The top ranked complex, as revealed by Glide score, was considered for ligand based validation based on its ability in reproducing a binding mode consistent with experimental and mutagenesis data.[44]

Pore Analysis. The pore radius together with shape and regularity were analyzed using the HOLE[45] program, which employs a Monte Carlo simulated annealing procedure to find the best route for a sphere with variable radius to squeeze through the channel. The conductance profile of the channel was also calculated using a simple Ohmic conductance model in the presence of 1(M) KCl as electrolyte to ensure if the models could be discriminated based on the conductance state. Electrostatic surface potential mapping and solvent accessible surface area calculation were carried out for both the ionophore complexes using APBS 1.3,[46] APBSmem 1.11,[47] and DrawMembrane. Input files for APBS were assigned with radii and charges information using PDB2PQR 1.7.[48]

APBS calculations were carried out using the Nonlinear Poisson–Boltzmann equation[49] with multiple Debye–Hückel boundary conditions. All the calculations were performed on a grid of size 289 × 161 × 161 with solvent probe radii of 1.4 Å at 298.15 K. A bathing solution of 0.15 M ionic concentration was used, which was composed of sodium and chloride ions with probe radii of 0.95 Å and 1.68 Å, respectively. A dielectric value of 2 was assigned for the protein, 78.5 for the solvent, and 2 for the membrane, while a dielectric value of 10 was assigned for the pore region. Visualization of the electrostatic potential and solvent accessible surface area results were carried out using PyMOL.[50]

Electrostatic Energy Profile of the Ion Channel Using Poisson–Boltzmann Methodology. The finite-difference Poisson–Boltzmann methodology implemented in APBS[46] was applied to calculate the solvation energy of a Cl^- ion by moving it through the channel pore from the N-terminal side (N-side) to the C-terminal side (C-side) of the channel. Linear PB equations were solved on an automatically configured sequential focusing grid of dimension 289 × 161 × 161. Input PQR files were generated as mentioned in the previous section. PoreWalker,[51] another program close in spirit to HOLE, was employed to find the coordinates of the central pore axis along the X axis. The influence of the membrane was included as a low-dielectric slab with a dielectric value $\epsilon_m = 2$, and the solute and solvent were assigned values of $\epsilon_p = 2$ and $\epsilon_w = 78.5$, respectively. A multiple Debye–Hückel boundary condition was employed, and the ionic concentration was set at 0.15 M. The modeled ion channel was centered at the origin with the pore aligned along the X axis of the Cartesian coordinate system. The permeating ion was treated explicitly using a univalent point negative charge emulating a chloride ion, with a radius of 1.68 Å. The change in solvation free energy, experienced by the ion at each point when moving from the bulk solvent phase to the pore of the channel, was sampled at discrete positions within spacing of 1 Å, and the energy was evaluated using the equation.

$$\Delta E_{PB} = (E_{complex} - E_{ion} - E_{protein})$$

Elastic Network Modeling (ENM) and Normal Mode Analysis (NMA). Allosteric transitions that regulate channel gating occur on a microsecond to millisecond time scale. Exploring such large scale conformational changes in a high dimensional space on a millisecond time scale is generally inaccessible using standard all atom molecular dynamic simulations. As a viable alternative, we employed a simplified yet effective coarse gained method termed Elastic Network Model (ENM).

Elastic network modeling treats proteins as networks of coupled harmonic oscillators and masses representing the starting structure. Analytical solutions obtained from ENM yields a basis set of orthogonal independent motions. An ENM model was constructed using the NOMAD-Ref server.[52] A distance weight of 5 Å was employed to obtain a smoother cutoff value. A contact cutoff of 8 Å, considering the size of the system, was introduced for defining the interactions. Conventional ENM approaches only consider Cα atoms, but the implementation of the rotation translation block (RTB) in NOMAD-Ref server ensured a full all-atom representation, and the modes obtained represent a linear combination of the rotations and translations of these blocks. The Hessian matrix was solved and diagonalized using the "Automatic" matrix solver option, and the first 10 lowest frequency normal modes and six modes that correspond to rigid body motions were computed.

One to one comparison of the normal modes obtained for the two different states (closed and open) were computed to quantify the degree of similarity of the conformational change and to ascertain if the captured global motions exhibit a collective character, which are more likely to be functional motions.

The overlap coefficients were computed for the first 106 lowest frequency modes of the two forms (open and closed) using the NOMAD-Ref server. The difference vector thus obtained between the two reference states represents the degree of overlap of the motion.

Normal modes thus generated were used to capture the biologically relevant motions. The tilt angle (τ) was calculated assuming an ideal helix. The tilt angle was defined as the angle subtended between the membrane normal and the helical axis of pore facing M2 helix. The rotation angle along the central pore axis was defined as the angle formed at the invariant center of mass of pore, between the reference M2 helix and the rotated

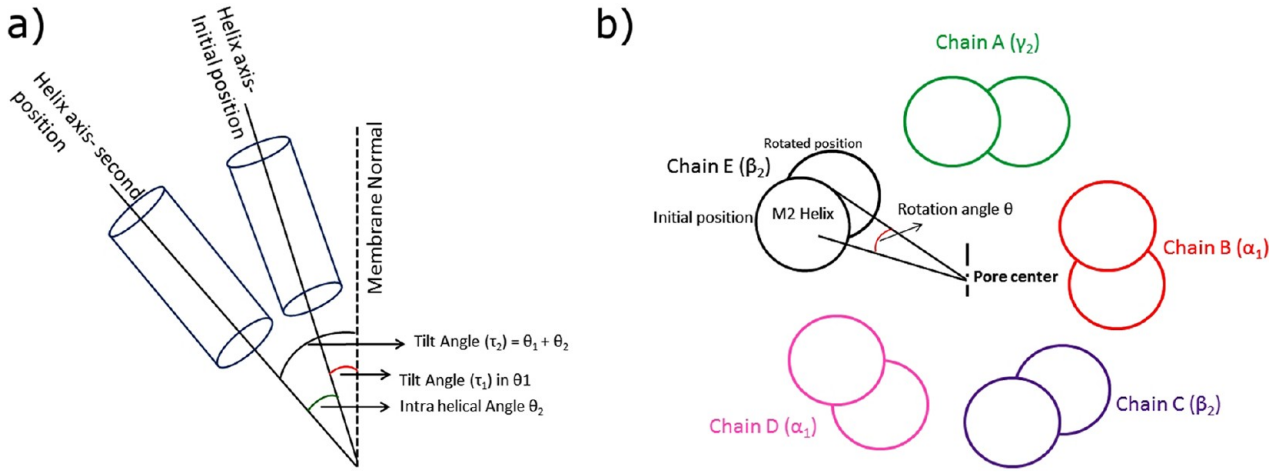

Figure 1. Schematic representation of (a) tilt angle (b) rotation angle calculation.

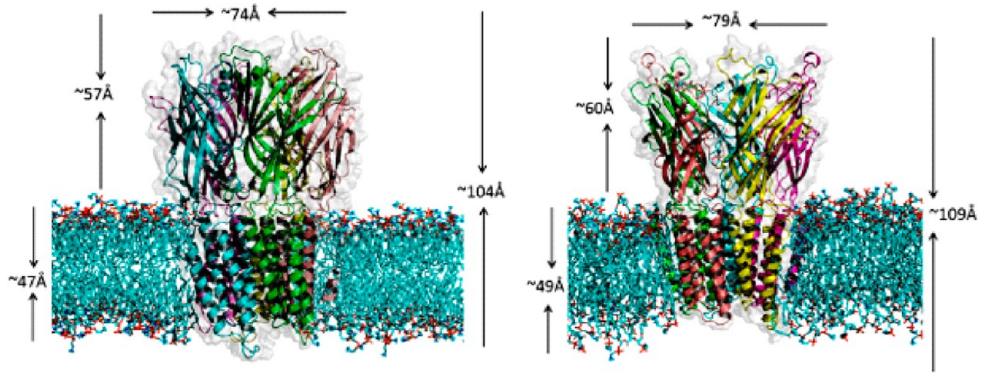

Figure 2. The left panel represents the closed state conformation and the right panel represents the open state conformation of the $GABA_A$ ion channel. The length of LBD and TM regions are highlighted together with the diameter values represented in Å. A lipid bilayer encompassing the trans membrane region is shown for aesthetic representation.

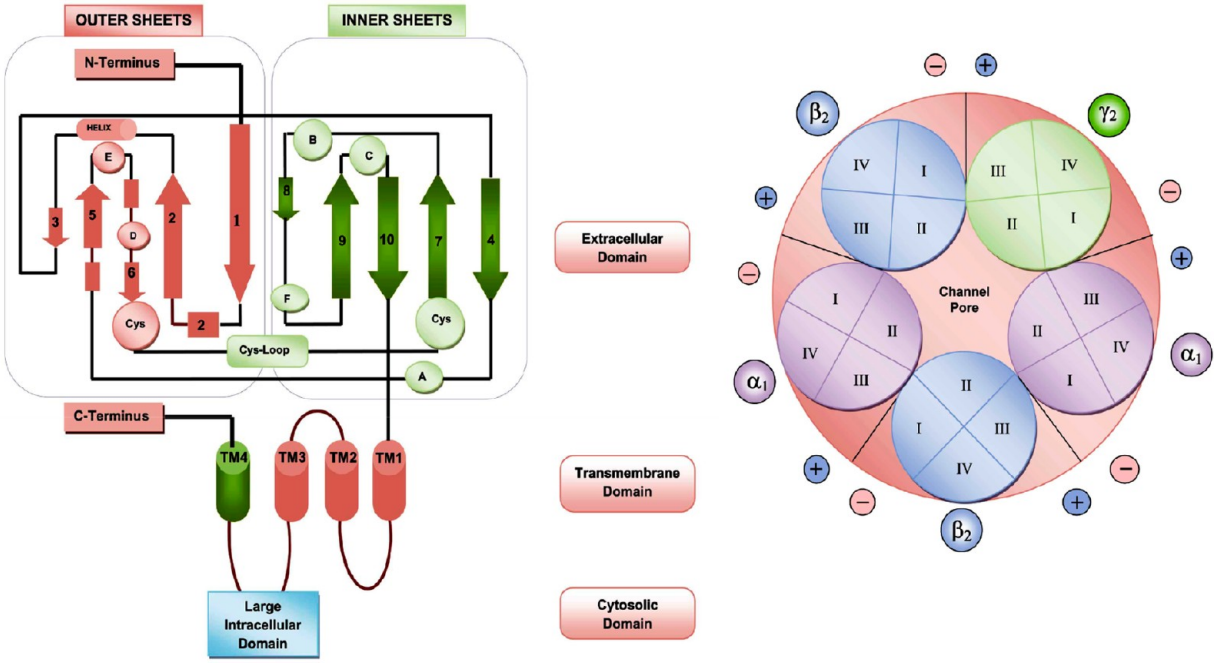

Figure 3. Left side panel: The topology of the $GABA_A$ subunit. Right side panel: Subunit stoichiometry and arrangement of $GABA_A$ receptor as evident from the modeled structure. The secondary structures were assigned using the DSSP algorithm.

dx.doi.org/10.1021/ci300189a | J. Chem. Inf. Model. 2012, 52, 2958−2969

position of the M2 helix. These calculations are pictorially represented in Figure 1.

Prior to the calculation of the tilt (τ) and the rotation angle the TM2 domains were aligned to the Z axis, and the coordinates were projected to the XY plane using the Orient option of VMD.[53]

RESULTS AND DISCUSSION

Structural Validation of the Homology Models. The topological properties of the modeled proteins (closed and open state) were analyzed to probe if the modeled proteins share a common architecture, known to be conserved among the Cys-loop receptors. The modeled structure reveals a topological architecture similar to those defined by the X-ray structure of the nACh receptor.[8] The length and dimension of the modeled $GABA_A$ receptor is pictorially represented in Figure 2.

A topological representation of the modeled $GABA_AR$ is shown in Figure 3. It was evident that the extracellular domain consists of a short α helix at the top followed by ten highly twisted β-strands, suggestive of a modified immunoglobulin like topology. The β-strands (numbered 4, 7, 8, 9, and 10) face the luminal or inner face, while the others (numbered 1, 2, 3, 5, and 6) face the abluminal or outer side. The sixth and seventh β-strands are connected by the signature disulfide bridge.

The 'plus−minus' interfaces of α_1+/γ_2- for BZD binding and α_1-/β_2+ for the GABA binding site, evident from the modeled proteins, imply that the transducing elements make use of these cross-connections.

The extracellular domain forms the vestibular pore, which tapers to form a narrow channel region (ion conductance pore) which is present well within the transmembrane region. It is evident from modeling that the four sets of helices M1 to M4 are equivalent to the previously described transmembrane regions in the pLGIC family. The M2 helices form the wall of the pore, whereas the fourth helix, M4, is located at the periphery. The M4 helix loosely interacts with M1 and M3 helices and is not involved in any subunit−subunit interactions. These findings imply that the modeled open state and closed state conformations of $GABA_AR$ have indeed captured many of the key conserved topological features typical of the pLGIC super family. Subsequently, the modeled structures were also evaluated for stereochemical accuracy, fold reliability, and packing quality using Procheck, Profile-3D, and Whatif. Profile-3D overall self-compatibility scores for the models were much higher than the lowest possible scores conceivable for such a model. Similarly, the PDF (pseudoenergy objective function) values, obtained from Modeller, were found to be well within the tolerable limits for both the models. No gross misfolded regions were observed, as evident from the Profile-3D plot (SI 3) and a residue-by-residue energy assessment carried out using the Discrete Optimized Protein Energy (DOPE) score. The Ramachandran plot (SI 4) of the $\Phi-\Psi$ angle distribution revealed that only 0.7% of the residues fall in the disallowed region for both the closed and open state models. The model validation parameter values are provided in Table 2.

We have carried out MD simulations of the protein−membrane−water system, consisting of about 400,000 atoms, for both the states for 5 ns each to understand stabilities of the systems and the accuracy of the modeling procedure. The overall structural stability of the two modeled states was verified by means of MD based root-mean-square deviation calculation (figure given in SI 5). MD based RMSD calculation has been previously reported to be a good indicator of structural quality for membrane proteins.[54] Analysis of backbone RMSD versus time reveals that the closed state is well equilibrated after 3 ns. While for the open state, RMSD shows the trend of continuous rise. This result is well expected, as the open structure will tend to move from open state to closed state during simulation time, and, in order to capture the full structural changes, microsecond time scale simulation is needed. That would be the part of our future communication.

Table 2. Model Validation Parameters Obtained for the Models

validation parameter	values (open)	values (closed)
PDF total energy[a]	−26494.08	−32240.31
$\Phi-\psi$ violations[b]	0.7%	0.7%
Profile-3D[c]	513.831	446.441
DOPE score[d]	−182368.09	−181936.89

[a]A pseudo energy function obtained from Modeller. [b]Percentage of residues lying in the disallowed region. [c]The minimum possible scores for the models are 311.34 and 325.56 for closed and open, respectively. [d]A statistical potential function for predicting errors in modeled proteins.

The ability of the modeled protein in reproducing realistic binding modes, consistent with known experimental evidence, is a *sine qua non* for a good model. A flexible docking approach (IFD), which remodels the active site based on the docked ligand, was able to produce a realistic binding mode for the orthosteric site ligand GABA. Ligplot[55] nonbonded interaction maps as evident from the docked binding mode of GABA are shown in Figure 4.

From the docked binding mode it is obvious that the anionic part of GABA interacts with the positively charged guanidino group of α_1Arg67. Indeed, earlier experimental studies involving single channel recording and kinetic modeling studies carried out after mutating arginine to alanine have revealed that α_1Arg67 and β_2Arg207 are critical residues required for stable binding of GABA.[56] α_1 R120K mutation has also underscored the essential role of arginines in GABA binding.[57] Interestingly, the IFD docking simulation reveals the intact salt bridge, evident in the tensed state between β_2Glu155 of the $\beta_2-\beta_2$ linker region and β_2Arg207 of the terminal β_{10} sheet belonging to the β_2 subunit, to be broken upon GABA binding. Postdocking of GABA, we find the amino part of GABA is involved in an H bonding interaction with the side chain carboxyl of β_2Glu155, thereby breaking the salt bridge interaction with β_2Arg207. A morphed movie of induced fit docking, based on the initial and the final docked states, is provided in SI 6. Indeed this observation is reminiscent of an earlier crystallographic finding in nAChRs, which has proposed the said structural change as the principal pathway leading to gating.[58] Incidentally, mutational studies have also suggested β_2E155C mutation to spontaneously open $GABA_A$ ion channels.[44] Molecular docking to the open conformation was also carried out. Glide XP docking produced binding modes were not consistent with mutagenesis and sulfhydryl-specific cross-linking experiments (shown in SI 7). This finding substantiates the state dependent binding of GABA and the kinetic model of GABA binding. The binding event which takes place in the closed state determines the rate constant (K_{on}), and the unbinding event in the open state drives the rate constant (K_{off}) and the affinity constant, $K_d = K_{on}/K_{off}$.

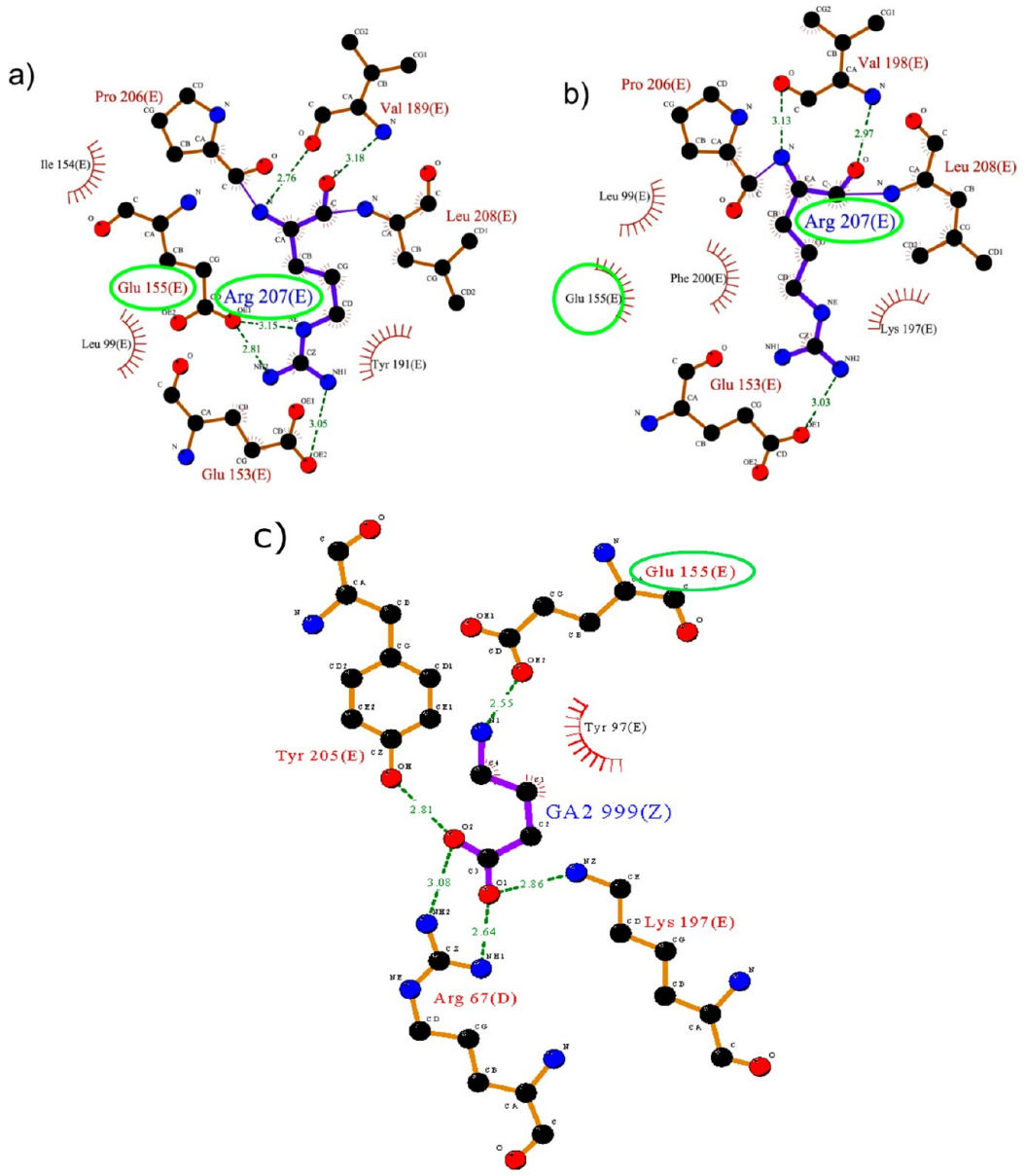

Figure 4. a) Closed state conformation of the $GABA_A$ ion channel with an intact inter-residual salt bridge interaction (between Glu155 (β_2) and Arg207 (β_2)) signifying a "tensed state". b) Open state conformation signifying the absence of the salt bridge interaction between Glu155 (β_2) and Arg207 (β_2) in chain E signifying a "relaxed" state. c) Complex obtained by induced fit docking of GABA revealing the loss of the inter-residual salt bridge interaction apparently signifying a transition from "tensed" state to "relaxed" state.

These observations, captured from the modeled structure, illustrate the ability of the model in reproducing reliable binding modes and exemplify the quality of the homology model from a ligand centric approach.

Upon validation of the models, the conducting states of the respective models were established to ascertain if the modeled structures represent the intended biophysical states. The conducting states of the modeled structures were initially established based on a simple Ohmic model. A high anion flux of around 1200 pS/M for the open state in contrast to a value of 1.9e-6 pS/M in the closed state affirms that the modeled structures reflect the conductance profile evinced in the respective states. We, however, did not notice any movement of ion through the pore during MD simulations for 5 ns, as such movement may require large time scale simulations.

APBS calculations were carried out to map the electrostatic potential of the ionophore complex. Predominant positive potential was observed for the closed state with regions clearly showing negative potential corresponding to the two constrictions, pinpointing the electrostatic barrier to Cl^- ion passage. A totally positive potential was observed for the pore lumen in the open state, which arises from the occupancy of basic amino acids, moving toward the ionic pore and thus providing an attractive environment to allow the Cl^- ion conductance. The electrostatic potential map for the pore lining residues is shown in Figure 5.

Thus the modeled closed and open state conformations allow discrimination, based on the electrostatic potential, and rationalize the anion selectivity of the channel.

Relating Structure to Function. Structural comparison of the modeled open and closed state conformations of the

dx.doi.org/10.1021/ci300189a | J. Chem. Inf. Model. 2012, 52, 2958−2969

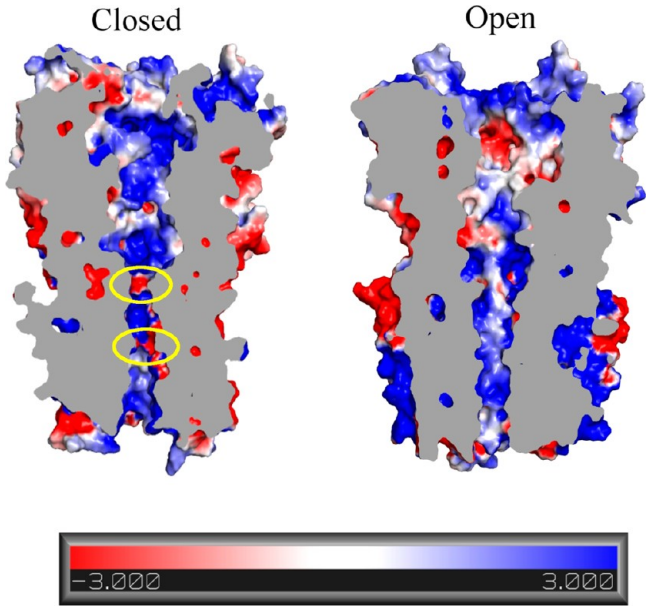

Figure 5. Equi-potential solid surface and color mapping of the electrostatic potential scaled at −3 and +3kT/e for the closed and open state. Blue (positive), white (neutral), red (negative). Encircled areas represent electrostatic barrier for Cl^- in the closed state. The figure represents the electrostatic profile for channel pore, rendered in the slab mode.

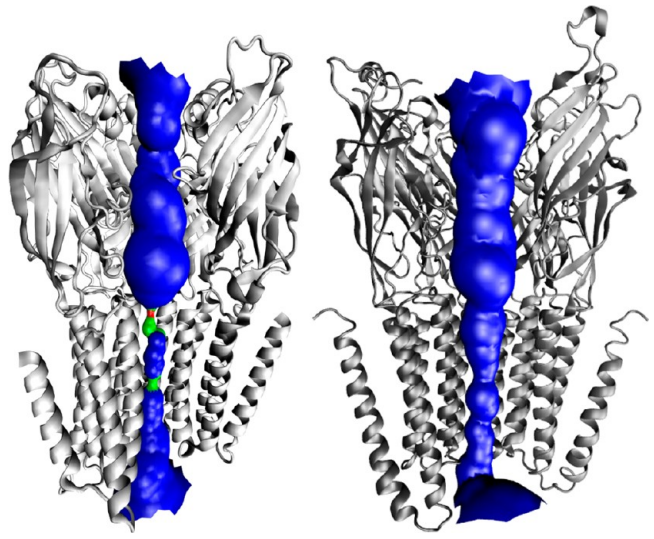

Figure 6. Channel visualization for closed (left), open (right) conformations.

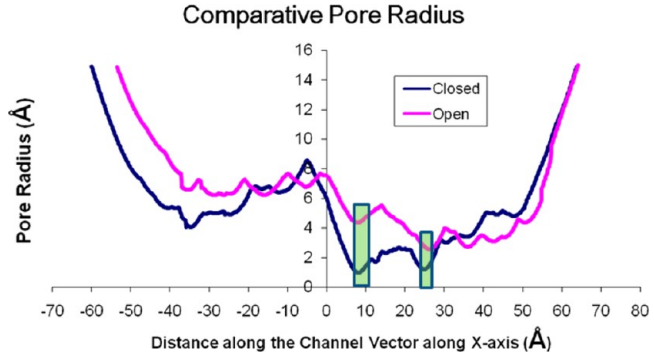

Figure 7. Comparative pore radius plot for the closed and open states of the $GABA_A$ ion channel at a given distance along the channel pore axis. The green bars represent the selectivity filter and the hydrophobic griddle regions.

$GABA_A$ ion channel was undertaken after an optimal structural alignment carried out using PyMOL. Conformational differences, evident in the models, exemplify the distinct conformation of the ion conduction state of the $GABA_A$ ion channel. The overall architecture reveals conserved secondary structural elements largely at the global level as shown in Figure 2. The only secondary structure change seen in the extracellular ligand binding domain of the open state conformation is the absence of the short 3_{10} helix near the N terminal α helix. This secondary structure change is attributed due to the inherent bias introduced by the template 2VLO which has a short 3_{10} helix that is absent in crystal structure 3EAM. This structural difference has been translated into the homology model. Loops intervening β sheets 1−2 and β sheets 8−9 display distinct conformations. Previous experimental studies have also indicated that these loops are dynamically coupled to the M2-M3 linker.[59] Thus the difference in the orientation of these loops implies a direct link to the conduction state of the ion channel as they are known to serve as the linking elements between the ECD and the TM region.

The pore structure for the open state model indicates a regular funnel shaped structure; on the contrary the closed state exhibits an irregular funnel shaped structure (Figure 6). In both the closed and the open state conformations, the vestibular pore had a maximum radius of around 16 Å (Figure 7). A clear consensus on the location of the gate seems to be elusive with different experimental studies hinting toward varied locations. Mutational studies have pointed toward the presence of a gate formed by a conserved ring of leucines and valines closer toward the beginning of the trans membrane region.[60] On the contrary, SCAM studies point toward the presence of a gate near the intracellular end (cytoplasmic end).[61] The cryo EM structure of Unwin[8] points toward the presence of a gate at the middle of the lipid bilayer resulting from a "hydrophobic griddle". In the present homology model we find two constrictions one closer toward the extracellular end and the other at the middle of the TM region (Figure 6).

The calculated pore radius for the closed and the open states are shown in Figure 7. The radius of the internal pore clearly indicates two distinct regions that essentially correspond to the selectivity filter and the hydrophobic griddle region (highlighted as the green bars in Figure 7). The calculated pore radius for the closed form at the sites of constriction is ∼1.0 Å. This value is significantly different in relation to the open form.

Pore radius calculation has also been used to validate the stability of the closed state structure at the level of pore lumen, during molecular dynamics simulation. The MD simulation based average structure of the closed state (generated from production run of 3 to 5 ns) was compared with the homology modeled structure of the same state (figure shown in SI 8). The plot clearly shows that the pore radius at the selectivity filter and the hydrophobic griddle regions is almost constant and holds the necessary structural stability.

A deeper analysis of these constrictions was carried out to map these sites at the residue level. The first constriction A (in Figure 8a) at the 20′ level (Lys285(A), Asn274(B), Glu270(C), Asn274(D), and Glu270(E)), which involves two rings of negatively charged residues, may hold a positive ion, thereby acting as a cation barrier and rendering it anion selective.

dx.doi.org/10.1021/ci300189a | J. Chem. Inf. Model. 2012, 52, 2958−2969

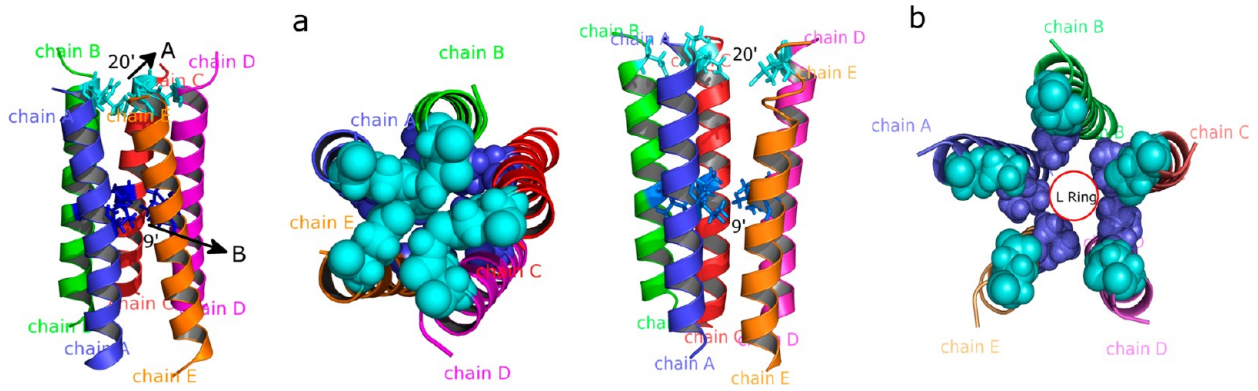

Figure 8. Transmembrane region of the ion channel depicting the closed (a) and the open (b) state as shown sideward and as viewed from the top of N terminal. 'A' First constriction formed by Lys285(A), Asn274(B), Glu270(C), Asn274(D), and Glu270(E) at the 20′ level. 'B' Second constriction formed by Leu274(A), Leu263(B), Leu259(C), Leu263(D), and Leu259(E) at the 9′ level. Only the pore facing M2 helixes of all the subunits are shown for clarity.

Previous studies have shown that reducing or reversing the charge on the 20′ region of the nACh receptor led to outward rectification of the channel.[62,63] Constriction around Glu270-(C) at 20 Å reveals an overall negative electrostatics, as evident from the Poission−Boltzmann electrostatic calculation (see Figure 5).

We believe that this negatively charged electrostatic environment defines the ionic selectivity profile of the channel. Poission−Boltzmann energy profile calculations for a Cl^- ion reveals a maxima at this position corresponding to 58 kJ/mol, a value significantly higher to be easily overcome (Figure 9).

The second constriction B is formed at the 9′ level by a ring of leucines (L ring) at the middle of M2 (Leu274(A), Leu263(B), Leu259(C), Leu263(D), and Leu259(E)) (Figure 8b). The literature entails these conserved 9′ leucine residues as "gate keeper" residues.[64,65] Mutating these hydrophobic residues to polar residues in neuronal nicotinic receptor alpha7 has resulted in a decreased rate of desensitization.[66] Our modeling study reinforces the "hydrophobic griddle" hypothesis.[8] It is speculated that these hydrophobic residues, lining the pore, would impede ion permeation by a process termed "hydrophobic gating". Electrostatic free energy profiles of the Cl^- ion quantified using the Poission−Boltzmann calculation reveal a relatively high energy barrier of 58 kJ/mol in the closed state over −137 kJ/mol for the open state. The desolvation energy barrier quantified using the Poission−Boltzmann calculation reveals a relatively high energy barrier of 58 kJ/mol in the closed state over −137 kJ/mol for the open state. Desolvation energy values considered together with the pore radius (∼1 Å in closed form (Figure 7)) clearly reveals that the Cl^- ion has to be stripped of the water molecules from its hydration shell if it were to pass this constriction. Such a process involves a large amount of desolvation free energy and will definitely prove to be a functional barrier for the permeation of a 1.81 Å radius Cl^- ion. The MD based free energy estimation using PMF as employed by the Sansom group and the FEP based method as employed by the Roux group would provide a rigorous test for this hypothesis.

The "hydrophobic griddle" is formed as a result of side chain packing interaction, because in the open state these hydrophobic L ring residues are directed inward, whereas in the closed conformation, they engage in a side chain to side chain packing interaction thereby helping to seal the ion pore (constriction B in Figure 8a).

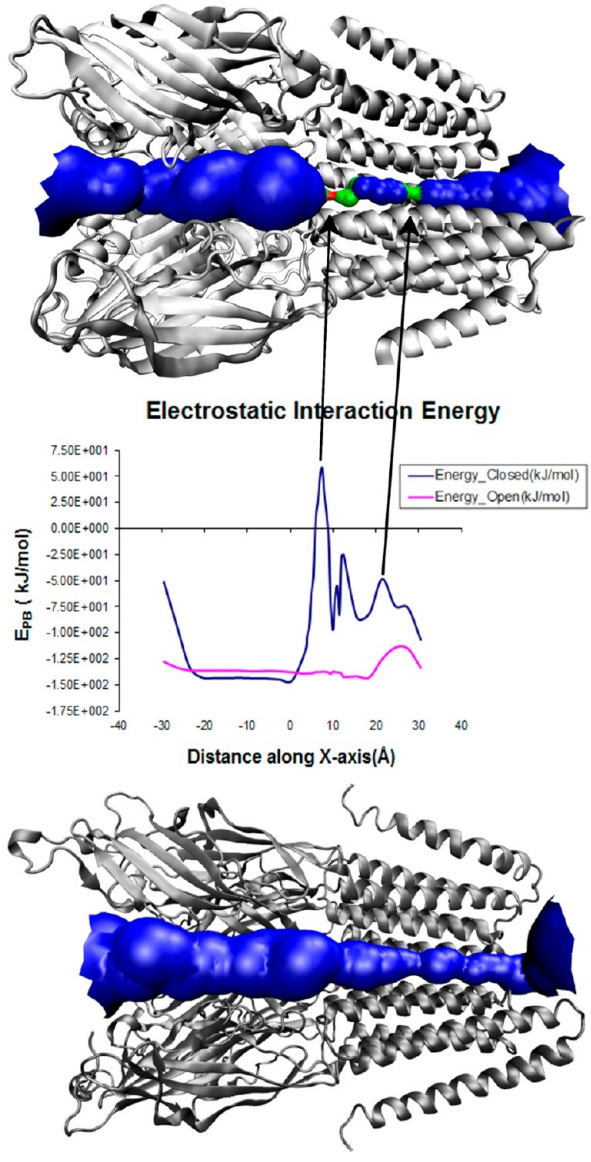

Figure 9. Electrostatic free energy profile for a chloride ion encountered at the central pore sampled every 1 Å is mapped onto the 3D coordinates.

dx.doi.org/10.1021/ci300189a | J. Chem. Inf. Model. 2012, 52, 2958−2969

Elastic Network Based Normal-Mode Analysis Captures the Gating Transition. Functionally relevant motions, captured from elastic network based NMA, are known to display a larger degree of correspondence with those obtained from principal components (PCA) analysis of MD trajectories or a classical force field based NMA approach.[67]

The low frequency modes obtained from an elastic network based NMA reveal a "Twist to Turn" type of quaternary motion. Ligand binding domain rotates counterclockwise around the central axis, and the transmembrane domain rotates in a clockwise fashion when viewed from the top. Low frequency normal modes are expected to display collective characters, especially when related to a functionally relevant conformational change. Henceforth, we decided to ascertain the degree of similarity between the direction of a chosen conformational change and the direction of a given normal mode for the closed state and the open state. The overlap measures projected in Figure 10 tend to reveal that the displayed "Twist to Turn" type of global motion exhibits a collective character.

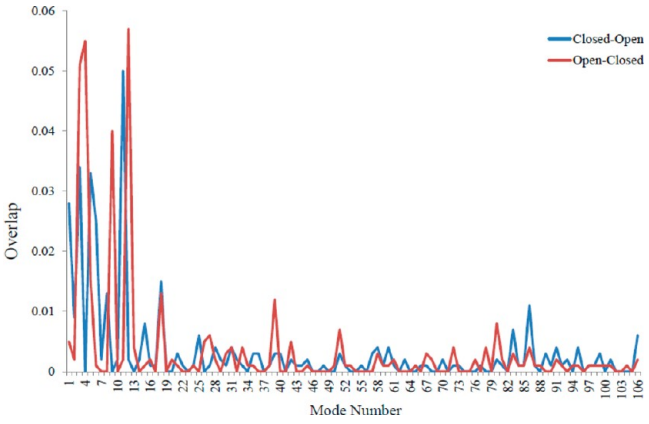

Figure 10. Overlap between a set of low frequency modes generated for the closed and the open state signifying a high degree of overlap.

This finding strongly hints that the "Twist to Turn" type of collective motion at the quaternary level could be strongly related to a $GABA_A$ channel gating.

The evinced "Twist to Turn" type of quaternary motion accompanies a deformation of the luminal β sandwich resulting from a downward pull of the β-sheets together with a tilting motion of the TM helices. The global motion captured by NMA is rendered in a movie and provided vide SI 9. We also find that the LBD domain of the pentamer and the TM helices undergo two types of rigid body rotational motions, one with respect to the subunit and the other with reference to the pore axis. The rotatory and tilting motion of the M2 helices results in widening and narrowing of the pore. Helanal[68] classifies M2 helix as a "Curved" helix, and no obvious kink was evident. Helical parameters like tilt and rotary angle for the M2 helices were calculated. The tilt angle calculated for all the pore facing M2 helices reveal a nonuniform tilting motion. Tilt angles and the rotary motion angle values are provided in Table 3.

It is speculated that this rotational motion helps in moving the bulky side chains of the residues, which point toward the lumen of the pore, when undergoing gating transition. The rotations of the M2 helices are asymmetrical in nature. The gating transition mechanism inferred using an elastic network based NMA approach is in broad agreement with a 1 μs molecular dynamics simulation study,[69] carried out on the crystal structure of GLIC, and other previous NMA studies[70,71] carried out on other pLIGIC. This principal observation implies that the mechanics involving pore opening and channel gating to be largely conserved among pLGIC. The large scale allosteric transition that occurs from closed to open state is largely reminiscent of an enthalpy driven type III type of allosteric mechanism. Such a type of allosteric signaling propagates through a series of discrete conformational changes both at the tertiary level (rewiring of residue − residue contact) and the quaternary level (collective, rigid-body motions).

Table 3. Tilt Angles and Rotatory Motion Angles for the M2 Helices

parameter	M2 chain A	M2 chain B	M2 chain C	M2 chain D	M2 chain E
tilt[a]	2.643–8.563	0–3.16	0–4.14	0–3.85	0–3.43
rotation[b]	12.64	11.71	11.29	11.61	12.11

[a]Signifies the minimum and the maximum tilt angle from the membrane normal. [b]Signifies the average rotation angle of the M2 helix.

CONCLUSION

The lack of structural data on the closed and open state of $GABA_A$ prompted us to undertake modeling studies based on the recently resolved X-ray crystallographic structures of two structural homologues. The present study helps to advance our understanding of the structure function relationship of the $GABA_A$ ion channel at an atomic level as the modeled structures are consistent with many experimental findings. ENM coupled with NMA helps in delineating the transition pathway from closed to the open conformation. Such coarse grained modeling offers the advantage of capturing large scale conformational changes that generally occur at a microsecond time scale. The overall structural topology, pore architecture, ionic selectivity profile, and conduction state of the homology models are largely reminiscent of pLGIC, and, hence, it establishes itself as an excellent framework for not only understanding the structural basis of neuronal inhibition but also for investigating channel modulation by allosteric modulators.

Beforehand assessment of the requisite validation parameters, inclusive of a ligand based validation approach, was undertaken to ensure the quality of the models. The Induced Fit Docking (IFD) protocol, employed for the said purpose, was able to simulate the breaking of the salt bridge interaction evident between Glu155(β_2) and Arg207(β_2) in the closed state, which is subsequently broken upon GABA binding (open state). The ability of the induced fit docking in reproducing realistic binding modes, consistent with experimental data, reinforces the quality of the homology model. The conducting states of the modeled structures were determined using a simple Ohmic model. The ability of the Ohmic model in discriminating structures, based on the conducting state, quantifies the ability of the models in capturing its relevant biophysical state. To illustrate how a conducting state of the channel alters the electrostatic environment across the lumen of the pore, we carried out an electrostatic surface potential mapping calculation employing the nonlinearized Poission–Boltzmann method. The change in electrostatics from an electronegative potential (found at the two constrictions) to the electropositive

dx.doi.org/10.1021/ci300189a | J. Chem. Inf. Model. 2012, 52, 2958–2969

(open) potential at the lumen during transition is attributed to an excess occupancy of basic amino acids that move toward the lumen of the pore in the open state, thereby providing an attractive environment for the conduction of the Cl^- ion. The ionic desolvation profile for a chloride ion propagating through the central pore axis was carried out, using APBS. The calculated solvation free energy reveals a free energy transfer value of 58 kJ/mol for the closed state against a value of −137 kJ/mol for the open state, around the selectivity filter region, and implies a strong electrostatic repulsion for an incoming chloride ion.

A coarse grained simulation using an elastic network formalism followed by Normal Mode analysis (NMA) was carried out to understand functionally relevant motions that facilitate channel gating. Low frequency modes obtained from NMA were reflective of the quaternary twisting motion that has been envisaged as the allosteric model for channel gating in pentameric ligand gated ion channel (pLGIC), a strong indication of a conserved gating mechanism among pLGIC.

■ ASSOCIATED CONTENT

Ⓢ Supporting Information

Additional details of the templates used and its structural criteria employed for selection are provided in SI 1. Target-template(s) sequence alignment is provided in SI 2. Profile 3D plots for closed and open models are provided in SI 3. The Ramachandran plots for closed and the open state models are provided in SI 4. The RMSD plots obtained from MD simulation for the closed and the open state models are given in SI 5. A morphed movie of induced fit docking is provided in SI 6. Results of docking $GABA_A$ to the open conformation are provided in SI 7. Comparison of the pore radius change observed between the molecular dynamics averaged structure of $GABA_A$ closed model and initial homology model structure of $GABA_A$ closed is provided in SI 8. The global motion captured by NMA is rendered in a movie and provided in SI 9. This material is available free of charge via the Internet at http://pubs.acs.org.

■ AUTHOR INFORMATION

Corresponding Author

*Phone: +91-33-2499-5700 (extn. 854/836). Fax: +91-33-2473-5197. E-mail: nghoshal@iicb.res.in. Corresponding author address: Structural Biology and Bioinformatics Division, CSIR-Indian Institute of Chemical Biology, 4 Raja S.C. Mullick Road, Jadavpur, Kolkata −700032, India.

Present Address

[‖]Center for Advanced Biotechnology and Medicine (CABM), 679 Hoes Lane, Piscataway, NJ 08854. USA.

Notes

The authors declare no competing financial interest.

■ ACKNOWLEDGMENTS

N.G. thanks CSIR, New Delhi for providing financial support. R.S.K.V. thanks the Council of Scientific and Industrial Research (CSIR) for a Research Associate Fellowship. M.P. thanks CSIR for a Senior Research Fellowship. I.B. and P.V.P. thank CSIR for a Project Fellowship. N.T. and S.N.R. thank the Ministry of Chemicals & Fertilizers for a scholarship. The authors thank Michael Grabe and Frank Marcoline for their help in running the APBSmem. Thanks are due to Dr. Nahren Manuel Mascarenhas for going through the manuscript.

■ REFERENCES

(1) Kuffler, S. W.; Edwards, C. Mechanism of gamma aminobutyric acid (GABA) action and its relation to synaptic inhibition. *J. Neurophysiol.* **1958**, *21*, 589−610.

(2) Rudolph, U.; Möhler, H. GABA-based therapeutic approaches: GABAA receptor subtype functions. *Curr. Opin. Pharmacol.* **2006**, *6*, 18−23.

(3) Bettler, B.; Kaupmann, K.; Mosbacher, J.; Gassmann, M. Molecular structure and physiological functions of GABA(B) receptors. *Physiol. Rev.* **2004**, *84*, 835−867.

(4) Korpi, E. R.; Gründer, G.; Lüddens, H. Drug interactions at $GABA_A$ receptors. *Prog. Neurobiol.* **2002**, *67*, 113−159.

(5) Mehta, A. K.; Ticku, M. K. An update on $GABA_A$ receptors. *Brain Res. Rev.* **1999**, *29*, 196−217.

(6) Schofield, P. R.; Darlison, M. G.; Fujita, N.; Burt, D. R.; Stephenson, F. A.; Rodriguez, H.; Rhee, L. M.; Ramachandran, J.; Reale, V.; Glencorse, T. A. Sequence and functional expression of the GABA A receptor shows a ligand-gated receptor super-family. *Nature* **1987**, *328*, 221−227.

(7) Ostermeier, C.; Michel, H. Crystallization of membrane proteins. *Curr. Opin. Struct. Biol.* **1997**, *7*, 697−701.

(8) Unwin, N. Refined structure of the nicotinic acetylcholine receptor at 4A resolution. *J. Mol. Biol.* **2005**, *346*, 967−989.

(9) Ernst, M.; Bruckner, S.; Boresch, S.; Sieghart, W. Comparative models of GABAA receptor extracellular and transmembrane domains: important insights in pharmacology and function. *Mol. Pharmacol.* **2005**, *68*, 1291−1300.

(10) O'Mara, M.; Cromer, B.; Parker, M.; Chung, S.-H. Homology model of the GABAA receptor examined using brownian dynamics. *Biophys. J.* **2005**, *88*, 3286−3299.

(11) Campagna-Slater, V.; Weaver, D. F. Molecular modeling of the GABAA ion channel protein. *J. Mol. Graphics Modell.* **2007**, *25*, 721−730.

(12) Vijayan, R. S. K.; Bera, I.; Prabu, M.; Saha, S.; Ghoshal, N. Combinatorial library enumeration and lead hopping using comparative interaction fingerprint analysis and classical 2D QSAR methods for seeking novel GABA(A) alpha(3) modulators. *J. Chem. Inf. Model.* **2009**, *49*, 2498−2511.

(13) Trudell, J. R.; Bertaccini, E. Comparative modeling of a GABAA alpha1 receptor using three crystal structures as templates. *J. Mol. Graphics Modell.* **2004**, *23*, 39−49.

(14) Bocquet, N.; Nury, H.; Baaden, M.; Le Poupon, C.; Changeux, J.-P.; Delarue, M.; Corringer, P.-J. X-ray structure of a pentameric ligand-gated ion channel in an apparently open conformation. *Nature* **2009**, *457*, 111−114.

(15) Hilf, R. J. C.; Dutzler, R. X-ray structure of a prokaryotic pentameric ligand-gated ion channel. *Nature* **2008**, *452*, 375−379.

(16) Uniprot Database. http://www.uniprot.org (accessed June 08, 2010).

(17) Altschul, S. F.; Gish, W.; Miller, W.; Myers, E. W.; Lipman, D. J. Basic local alignment search tool. *J. Mol. Biol.* **1990**, *215*, 403−410.

(18) Shi, J.; Blundell, T. L.; Mizuguchi, K. FUGUE: sequence-structure homology recognition using environment-specific substitution tables and structure-dependent gap penalties. *J. Mol. Biol.* **2001**, *310*, 243−257.

(19) Liu, H.-L.; Shu, Y.-C.; Wu, Y.-H. Molecular dynamics simulations to determine the optimal loop length in the helix-loop-helix motif. *J. Biomol. Struct. Dyn.* **2003**, *20*, 741−745.

(20) *Discovery Studio*, version 2.5; Accelrys: San Diego, CA, 2007.

(21) Sali, A.; Blundell, T. L. Comparative protein modeling by satisfaction of spatial restraints. *J. Mol. Biol.* **1993**, *234*, 779−815.

(22) MacKerell, A. D.; Bashford, D.; Bellott, M.; Dunbrack, R. L.; Evanseck, J. D.; Field, M. J.; Fischer, S.; Gao, J.; Guo, H.; Ha, S.; Joseph-McCarthy, D.; Kuchnir, L.; Kuczera, K.; Lau, F. T. K.; Mattos, C.; Michnick, S.; Ngo, T.; Nguyen, D. T.; Prodhom, B.; Reiher, W. E.; Roux, B.; Schlenkrich, M.; Smith, J. C.; Stote, R.; Straub, J.; Watanabe, M.; Wiórkiewicz-Kuczera, J.; Yin, D.; Karplus, M. All-atom empirical potential for molecular modeling and dynamics Studies of proteins. *J. Phys. Chem. B* **1998**, *102*, 3586−3616.

(23) Shen, M.; Sali, A. Statistical potential for assessment and prediction of protein structures. *Protein Sci.* **2006**, *15*, 2507−2524.
(24) *InsightII,* version 4.1; Accelrys: San Diego, CA, 2007.
(25) Laskowski, R. A.; MacArthur, M. W.; Moss, D. S.; Thornton, J. M. PROCHECK - a program to check the stereochemical quality of protein structures. *J. Appl. Crystallogr.* **1993**, *26*, 283−291.
(26) Vriend, G. WHAT IF: a molecular modeling and drug design program. *J. Mol. Graphics Modell.* **1990**, *8*, 52−56.
(27) Kabsch, W.; Sander, C. Dictionary of protein secondary structure: pattern recognition of hydrogen-bonded and geometrical features. *Biopolymers* **1983**, *22*, 2577−2637.
(28) Hess, B.; Kutzner, C.; van der Spoel, D.; Lindahl, E. GROMACS 4: Algorithms for highly efficient, load-balanced, and scalable molecular simulation. *J. Chem. Theory Comput.* **2008**, *4*, 435−447.
(29) Oostenbrink, C.; Villa, A.; Mark, A. E.; Gunsteren, W. F. A biomolecular force field based on the free enthalpy of hydration and solvation: the GROMOS force-field parameter sets 53A5 and 53A6. *J. Comput. Chem.* **2004**, *25*, 1656−1676.
(30) Berendsen, H.; Postma, J.; Gunsteren, W.; Hermans, J. Interaction Models for Water in Relation to Protein Hydration. In: *Intermolecular Forces*; Pullman, B., Ed.; D. Reidel Publishing Co.: Amsterdam, 1981; pp 331−342.
(31) http://moose.bio.ucalgary.ca/index.php?page=Structures_and_Topologies (accessed Jan 06, 2011).
(32) Nosé, S. A molecular dynamics method for simulations in the canonical ensemble. *Mol. Phys.* **1984**, *52*, 255−268.
(33) Parrinello, M.; Rahman, A. Polymorphic transitions in single crystals: a new molecular dynamics method. *J. Appl. Phys.* **1981**, *52*, 7182−7190.
(34) Darden, T.; York, D.; Pedersen, L. Particle mesh Ewald: an N.log(N) method for Ewald sums in large systems. *J. Chem. Phys.* **1993**, *98*, 10089−10092.
(35) Hess, B.; Bekker, H.; Berendsen, H. J. C.; Fraaije, J. LINCS: a linear constraint solver for molecular simulations. *J. Comput. Chem.* **1997**, *18*, 1463−1472.
(36) Evers, A.; Klebe, G. Ligand-supported homology modeling of protein binding-sites using knowledge-based potentials. *Angew. Chem., Int. Ed. Engl.* **2004**, *43*, 248−251.
(37) Evers, A.; Gohlke, H.; Klebe, G. Ligand-supported homology modeling of g-protein-coupled receptor sites: models sufficient for successful virtual screening. *J. Mol. Biol.* **2003**, *334*, 327−345.
(38) Katritch, V.; Rueda, M.; Lam, P. C.-H.; Yeager, M.; Abagyan, R. GPCR 3D homology models for ligand screening: lessons learned from blind predictions of adenosine A2a receptor complex. *Proteins* **2010**, *78*, 197−211.
(39) Radestock, S; Weil, T.; Renner, S. Homology model-based virtual screening for GPCR ligands using docking and target-biased scoring. *J. Chem. Inf. Model.* **2008**, *48*, 1104−1117.
(40) *Schrödinger Suite,* version 9.0; *Induced Fit Docking protocol*; Schrödinger LLC: New York, NY, 2008.
(41) *HyperChem*, version7.52; Hypercube: Gainesville, Fl, USA, 2002.
(42) Friesner, R. A.; Banks, J. L.; Murphy, R. B.; Halgren, T. A.; Klicic, J. J.; Mainz, D. T.; Repasky, M. P.; Knoll, E. H.; Shelley, M.; Perry, J. K.; Shaw, D. E.; Francis, P.; Shenkin, P. S. Glide: a new approach for rapid, accurate docking and scoring. 1. Method and assessment of docking accuracy. *J. Med. Chem.* **2004**, *47*, 1739−1749.
(43) Jacobson, M. P.; Pincus, D. L.; Rapp, C. S.; Day, T. J. F.; Honig, B.; Shaw, D. E.; Friesner, R. A. A hierarchical approach to all-atom protein loop prediction. *Proteins* **2004**, *55*, 351−367.
(44) Newell, J. G.; McDevitt, R. A.; Czajkowski, C. Mutation of glutamate 155 of the GABAA receptor 2 subunit produces a spontaneously open channel: a trigger for channel activation. *J. Neurosci.* **2004**, *24*, 11226−11235.
(45) Smart, O. S.; Neduvelil, J. G.; Wang, X.; Wallace, B. A.; Sansom, M. S. HOLE: a program for the analysis of the pore dimensions of ion channel structural models. *J. Mol. Graphics* **1996**, *14*, 354−360.
(46) Baker, N. A.; Sept, D.; Joseph, S.; Holst, M. J.; McCammon, J. A. Electrostatics of nanosystems: application to microtubules and the ribosome. *Proc. Natl. Acad. Sci. U.S.A.* **2001**, *98*, 10037−10041.
(47) Callenberg, K. M.; Choudhary, O. P.; de Forest, G. L.; Gohara, D. W.; Baker, N. A.; Grabe, M. APBSmem: A Graphical Interface for Electrostatic Calculations at the Membrane. *PLoS One* **2010**, *5*, e12722.
(48) Dolinsky, T. J.; Nielsen, J. E.; McCammon, J. A.; Baker, N. A. PDB2PQR: an automated pipeline for the setup, execution, and analysis of Poisson-Boltzmann electrostatics calculations. *Nucleic Acids Res.* **2004**, *32*, 665−667.
(49) Sharp, K. A.; Honig, B. Calculating total electrostatic energies with the nonlinear Poisson-Boltzmann equation. *J. Phys. Chem.* **1990**, *94*, 7684−7692.
(50) *PyMOL Molecular Graphics System*, version 1.3; DeLano Scientific: Palo Alto, CA, 2002.
(51) Pellegrini-Calace, M.; Maiwald, T.; Thornton, J. M. PoreWalker: a novel tool for the identification and characterization of transmembrane protein channels from their three-dimensional structure. *PLoS Comput. Biol.* **2009**, *5*, 1−16.
(52) Lindahl, E.; Azuara, C.; Koehl, P.; Delarue, M. NOMAD-Ref: visualization, deformation and refinement of macromolecular structures based on all-atom normal mode analysis. *Nucleic Acids Res.* **2006**, *34*, 52−56.
(53) Humphrey, W.; Dalke, A.; Schulten, K. VMD: visual molecular dynamics. *J. Mol. Graphics* **1996**, *14*, 33−38.
(54) Law, R. J.; Capener, C.; Baaden, M; Bond, P. J.; Campbell, J.; Patargias, G.; Arinaminpathy, Y.; Sansom, M. S. Membrane protein structure quality in molecular dynamics simulation. *J. Mol. Graphics Modell.* **2005**, *24*, 157−165.
(55) Wallace, A. C.; Laskowski, R. A.; Thornton, J. M. LIGPLOT: a program to generate schematic diagrams of protein-ligand interactions. *Protein Eng.* **1995**, *8*, 127−134.
(56) Goldschen-Ohm, M. P.; Wagner, D. A.; Jones, M. V. Three arginines in the $GABA_A$ receptor binding pocket have distinct roles in the formation and stability of agonist- versus antagonist-bound complexes. *Mol. Pharmacol.* **2011**, *80*, 647−656.
(57) Westh-Hansen, S. E.; Witt, M. R.; Dekermendjian, K.; Liljefors, T.; Rasmussen, P. B.; Nielsen, M. Arginine residue 120 of the human GABAA receptor alpha 1, subunit is essential for GABA binding and chloride ion current gating. *Neuroreport* **1999**, *10*, 2417−2421.
(58) Unwin, N.; Miyazawa, A.; Li, J.; Fujiyoshi, Y. Activation of the nicotinic acetylcholine receptor involves a switch in conformation of the alpha subunits. *J. Mol. Biol.* **2002**, *319*, 1165−1176.
(59) Gay, E. A.; Yakel, J. L. Gating of nicotinic ACh receptors; new insights into structural transitions triggered by agonist binding that induce channel opening. *J. Physiol.* **2007**, *584*, 727−733.
(60) Labarca, C.; Nowak, M. W.; Zhang, H.; Tang, L.; Deshpande, P.; Lester, H. A. Channel gating governed symmetrically by conserved leucine residues in the M2 domain of nicotinic receptors. *Nature* **1995**, *376*, 514−516.
(61) Akabas, M. H.; Kaufmann, C.; Archdeacon, P.; Karlin, A. Identification of acetylcholine receptor channel-lining residues in the entire M2 segment of the alpha subunit. *Neuron* **1994**, *4*, 919−927.
(62) Imoto, K.; Busch, C.; Sakmann, B.; Mishina, M.; Konno, T.; Nakai, J.; Bujo, H.; Mori, Y.; Fukuda, K.; Numa, S. Rings of negatively charged amino acids determine the acetylcholine receptor channel conductance. *Nature* **1988**, *335*, 645−648.
(63) Moorhouse, A. J.; Keramidas, A.; Zaykin, A.; Schofield, P. R.; Barry, P. H. Single channel analysis of conductance and rectification in cation- selective, mutant glycine receptor channels. *J. Gen. Physiol.* **2002**, *119*, 411−425.
(64) Unwin, N. Acetylcholine receptor channel imaged in the open state. *Nature* **1995**, *373*, 37−43.
(65) Labarca, C.; Nowak, M. W.; Zhang, H.; Tang, L.; Deshpande, P.; Lester, H. A. Channel gating governed symmetrically by conserved leucine residues in the M2 domain of nicotinic receptors. *Nature* **1995**, *376*, 514−516.

(66) Revah, F.; Bertrand, D.; Galzi, J. L.; Devillers-Thiéry, A.; Mulle, C.; Hussy, N.; Bertrand, S.; Ballivet, M.; Changeux, J. P. Mutations in the channel domain alter desensitization of a neuronal nicotinic receptor. *Nature* **1991**, *353*, 846−849.
(67) Case, D. A. Normal mode analysis of protein dynamics. *Curr. Opin. Struct. Biol.* **1994**, *4*, 285−290.
(68) Bansal, M.; Kumar, S.; Velavan, R. HELANAL: A program to characterise helix geometry in proteins. *J. Biomol. Struct. Dyn.* **2000**, *17*, 811−819.
(69) Nury, H.; Poitevin, F.; Van Renterghem, C.; Changeux, J.-P.; Corringer, P.-J.; Delarue, M.; Baaden, M. One-microsecond molecular dynamics simulation of channel gating in a nicotinic receptor homologue. *Proc. Natl. Acad. Sci. U.S.A.* **2010**, *107*, 6275−6280.
(70) Taly, A.; Delarue, M.; Grutter, T.; Nilges, M.; Le Novère, N.; Corringer, P.-J.; Changeux, J.-P. Normal mode analysis suggests a quaternary twist model for the nicotinic receptor gating mechanism. *Biophys. J.* **2005**, *88*, 3954−3965.
(71) Cheng, X.; Lu, B.; Grant, B.; Law, R. J.; McCammon, J. A. Channel opening motion of a7 nicotinic acetylcholine receptor as suggested by normal mode analysis. *J. Mol. Biol.* **2006**, *355*, 310−324.